Submicron aerosols at thirteen diversified sites in China: size distribution, new particle formation and corresponding contribution to cloud condensation nuclei production

J.F. Peng[1], M. Hu[1,*], Z.B. Wang[1,ǂ], X.F. Huang[2], P. Kumar[3, 4], Z.J. Wu[1], S. Guo[1], D.L Yue[1], D.J. Shang[1], Z. Zheng[1], L.Y. He[2]

[1]State Key Joint Laboratory of Environmental Simulation and Pollution Control, College of Environmental Sciences and Engineering, Peking University, Beijing 100871, China

[2]Key Laboratory for Urban Habitat Environmental Science and Technology, School of Environment and Energy, Peking University Shenzhen Graduate School, Shenzhen 518055, China

[3]Department of Civil and Environmental Engineering, Faculty of Engineering and Physical Sciences (FEPS), University of Surrey, Guildford GU2 7XH, United Kingdom

[4]Environmental Flow (EnFlo) Research Centre, FEPS, University of Surrey, Guildford GU2 7XH, United Kingdom

[ǂ]Now at: Multiphase Chemistry Department, Max Planck Institute for Chemistry, Mainz 55128, Germany

**Correspondence to:* M. Hu (minhu@pku.edu.cn)

Abstract

Understanding the particle number size distributions in diversified atmospheric environments is important in order to design mitigation strategies related to submicron particles and their effects on regional air quality, haze and human health. In this study, we conducted 15 different field measurement campaigns between 2007 and 2011 at 13 individual sites in China, including 5 urban sites, 4 regional sites, 3 coastal/background sites and one ship cruise measurement along eastern coastline of China. Size resolved

particles were measured in the 15-600 nm size range. The median particle number concentrations (PNCs) were found to vary in the range of 1.1-2.2 $\times 10^4$ cm^{-3} at urban sites, 0.8-1.5 $\times 10^4$ cm^{-3} at regional sites, 0.4-0.6 $\times 10^4$ cm^{-3} at coastal/background sites, and 0.5$\times 10^4$ cm^{-3} during cruise measurement. Peak diameters at each of these sites varied greatly from 24 nm to 115 nm. Particles in the 15-25 nm (nucleation mode), 25-100 nm (Aitken mode) and 100-600 nm (accumulation mode) range showed different characteristics at each sites, indicating the features of primary emissions and secondary formation in these diversified atmospheric environments. Diurnal variations show a build-up of accumulation mode particles belt at regional sites, suggesting the contribution of regional secondary aerosol pollution. Frequencies of new particle formation (NPF) events were much higher at urban and regional sites than at coastal sites and cruise measurement. The average growth rates (GRs) of nucleation mode particles were 8.0-10.9 nm h^{-1} at urban sites, 7.4-13.6 nm h^{-1} at regional sites and 2.8-7.5 nm h^{-1} at coastal sites and cruise measurement. The high gaseous precursors and strong oxidation at urban and regional sites not only favored the formation of particles, but also accelerated the growth rate of the nucleation mode particles. No significant difference in condensation sink (CS) during NPF days were observed among different site types, suggesting that the NPF events in background areas were more influenced by the pollutant transport. In addition, average contributions of NPF events to potential cloud condensation nuclei (CCN) at 0.2% super-saturation in the afternoon of all sampling days were calculated as 11% and 6% at urban sites and regional sites, respectively. On the other hand, NPF events at coastal sites and cruise measurement had little impact on potential production of CCN. This study provides a large dataset of particle size distribution in diversified atmosphere of China, improving our general understanding of emission, secondary formation, new particle formation and corresponding CCN activity of submicron aerosols in Chinese environments.

Key words: Submicron aerosols; Size distribution; New particle formation; Cloud condensation nuclei

1 Introduction

Atmospheric particles play an important role in the degradation of visibility and changing the balance of global radiative forcing (Dusek, 2006; IPCC, 2007), besides showing adverse impacts on human health (Heal et al., 2012). Size of atmospheric particles, ranging from 1.5 nm up to hundreds of micrometers, is a key factor for evaluating environmental effects of particles (*Kulmala et al., 2013*; *Buseck and Adachi*, 2008; *Kumar et al.*, 2014). For example, particle diameter is considered to be more important than chemical composition for cloud-nucleating ability (*Dusek*, 2006). Smaller particles may have greater potential of health impacts compared with their larger counterparts (*WHO, 2013*). Particles smaller than 100 nm in diameter (ultrafine particles) have deeper deposition in human body and are able to induce more intense oxidative stress in cells (*Nel et al.*, 2006). Accumulation mode particles, on the other hand, have high light extinction efficiency and can explain degradation of visibility in severe air pollution event to a great extent (*See et al.*, 2006). Meanwhile, particle size distribution offers information on type, origin, and atmospheric transformation of the particles (*Buseck and Adachi*, 2008; *Harrison et al.*, 2011). Therefore, the knowledge of size distributions of submicron particles, including their temporal and spatial variability, is crucial in characterizing human exposure, estimating climate effects, and designing monitoring strategies for both developed and developing countries (*Kumar et al.*, 2014).

Measurements of particle number distribution (PND) have been extensively conducted in many European and US sites in the past two decades (*Asmi, A. et al., 2011*; *Bigi and Ghermandi*, 2011; *Borsos et al.*, 2012; *Kumar et al.*, 2010; *Wehner and Wiedensohler*, 2003), but at a much lesser extent in developing countries (*Monkkonen et al.*, 2005; *Wu et al.*, 2008*; Kumar et al., 2011; Wang et al., 2013a,b*). Temporal and spatial variation of PND in these developed countries has been widely recognized (*Asmi, A. et al., 2011*). Whilst these particles arise from a number of non-vehicle exhaust sources (*Kumar et al.*, 2013b), primary emission from road vehicles is thought to be a main source of particle number concentration (PNC) in urban areas (*Kumar et al.*, 2010).

The new particle formation (NPF), associated with a rapid burst of nucleation mode particles, results in an increase of CCN number concentration after growth (*Wiedensohler et al.*, 2009). The NPF events were observed in many atmospheric environments in the world, especially in relatively clean atmosphere (*Kulmala et al.*, 2013). Though the first study on NPF events during polluted episodes was conducted in the megacity of Beijing (*Wehner et al., 2004; Wu et al., 2007*), the occurrence of NPF events is only reported at a few sites in China up to now (*Du et al.*, 2012; *Liu et al.*, 2008; *Wang et al.*, 2013c; *Wehner et al.*, 2004; *Wiedensohler et al.*, 2009; *Herrmann et al., 2014*). Although it is a common interest that regional NPF events are a main source of atmospheric CCN production (*Kuang et al.*, 2009), most of the estimation on the contribution of NPF events to CCN concentration till date are only based on model simulations using regional/global scale models with extra NPF mode (*Merikanto et al.*, 2009; *Yu et al.*, 2012). The only few measurement studies that attempted to quantify the strength of this nucleation process merely calculated the enhancement of CCN concentration along with NPF events (*Yue et al., 2011*; *Kerminen et al.*, 2012; *Kuang et al.*, 2009; *Asmi, E. et al., 2011*). These enhancment results are likely to be greatly influenced by factors such as change of boundary laryer as well as primary emissions. More measurements and new measurement-based approaches are therefore needed to estimate the contribution of NPF to corresponding CCN concentration in diversified environments.

China has been experiencing unprecedented modernization and urbanization process since 1980s. The rapid industrial revolution has intensively occurred in China during the past 30 years, providing both the chance to become “the world factory” and the challenge of severe air pollution problem. The aerosol pollution in recent years at both local and regional scale has attracted great attention, as it results in the heavy smog or haze episodes and might lead to potential health effects (*Xu et al.*, 2013). The aerosol pollution characterizes regional property in major economic developed regions with megacity or city clusters, for instance, Bohai Sea Rim Region, Yangtze River Delta and Pearl River Delta. To understand the feature of aerosol pollution in these regions

requires multi-site measurements within each pollution region.

In this study, we have therefore conducted PND measurements at 13 different sites in China in order to provide comprehensive understanding of the effects of primary emissions, regional pollutants transportation and new particle formation on PNDs. These sites are classified into four main categories – urban, regional, coastal and ship cruising – representing the typical atmospheric environments in China. Unique features of each site category, including the particle size distributions, seasonal and diurnal variation, are discussed in this paper. Special focus is given to the NPF events and their contribution to CCN concentration at each of the thirteen sites.

2 Methodology

2.1 Sites description

A total of 15 field measurement campaigns of PNDs were conducted at 13 different sites between 2007 and 2011. These sites were broadly classified in the following four types of atmospheric environment categories (see Table 1), including five urban sites, four regional sites, three coastal/ background sites and one ship cruise measurement along Eastern coastal China . As shown in Fig. 1, most of these sites were situated in the most developed and largest city cluster regions in China.

2.1.1 Urban sites

The first urban site, Guangzhou (GZ_u; 23.13˚ N, 113.26˚ E) was located on the roof of the Guangdong Provincial Environmental Monitoring Center in the downtown of Guangzhou city, at a height of about 50 m above street level (*Yue et al.*, 2013). This site is representative of a typical ambient condition in Guangzhou urban areas (*Zhang et al.*, 2008).

The second urban site, Shanghai (SH_u; 21.53˚ E, 31.23˚ N), was located on the roof of a 6-floor building of Shanghai Pudong Environmental Monitoring Station in the eastern part of Shanghai urban areas. The surroundings of this site were mainly residential and business buildings (*Huang et al.*, 2012).

The third urban site, Urumchi (UR_u; 87.58°N, 43.83°E), was located on roof of the Urumchi Environmental Monitoring Center in the downtown of Urumchi city. Urumchi city is the capital of Xinjiang Uyghur Autonomous Region, with the biggest desert in China to the north and mountains to the south. Sampling inlet at UR_u site was located at ~20 m above the street level. The surroundings were mainly residential and business buildings. There was one main road 200 m away to the west and another 400 m away to the east.

The fourth urban site, Wuxi (WX_u; 31.56° N, 120.29° E), was located on the roof of a five-floor building in the center of Wuxi City. This site was surrounded by the residential buildings. No obvious stationary sources existed nearby and the nearest main road was about 300 meters away to the east. The sampling inlet was at ~15 m above the ground level.

The fifth urban site, Jinhua (JH_u; 29.1 °N, 119.69 °E), was located on the roof of the Jindong Environmental Building in the east part of the city of Jinhua. The sampling inlet was at ~25 m above the street level. There was no industry source nearby and the nearest main road was located ~300 m away to the west. As the wind direction is always from northeast during the measurements (October), the influence of this main road on our site can be ignored.

2.1.2. Regional sites

The first regional site, Heshan (HS_r; 22.71 °N, 112.93 °E), was an urban outflow site of Guangzhou megacity in central Pearl River Delta (PRD), with a distance from Guangzhou downtown 50 km. It was located on the top of a small hill (40 m), about 7 km away from Heshan downtown areas, and was far from strong industrial sources. The surrounding areas of the site were dominated by farmlands and forests. Biomass burning events were observed occasionally in the farmlands. This site can be well representative of the air pollution outflow from the polluted central PRD urban areas (*Gong et al.*, 2012).

The second regional site, Kaiping (KP_r; 22.33 °N, 112.54 °E), was located ~120

km away from the city of Guangzhou to the southwest. Under the influence of the Asian monsoon, the dominant air mass comes to PRD from the northeast in fall. Hence, the Kaiping site could be assumed to be a downwind receptor site. Instruments were placed on the third floor of the building at the Kaiping supersite (~10 m above the ground level), which is surrounded by shrubs and eucalyptus forest (*Wang et al.*, 2013c). The site was free of any significant local pollution emissions. A detailed geographic description of this measurement site can be seen elsewhere (*Huang et al.*, 2011).

The third regional site, Jiaxing (JX_r; 30.8 ° N, 120.8 ° E), was a suburban site between Shanghai and Hangzhou. It was located on the roof of school building in a small town, 15 m above the ground level and 8 km away from the downtown of Jiaxing city, which was situated in the middle of Shanghai megacity and Hangzhou, capital of Zhejiang province.

The fourth regional site, Yufa (YF_r; 39.51 ° N, 116.3 ° E), was about 40 km to the south of Beijing downtown area. This site was located on top of a building (~20 m above the ground level) at the campus of Huangpu College. There was no industrial sources around this site, except the farm land and a residential area (*Guo et al.*, 2010).

2.1.3 Three coastal/ background sites

The first coastal site, Baguang (BG_c; 22.65 °N, 114.54 °E), was located on the roof of a three-floor building (~10 m above sea level) at the seaside in a small peninsula in the southern China, 50 km away from the city of Shenzhen to the east. No stationary source or traffic source was found nearby the site. To the east and south of the site was the South China Sea. This site can well represent the background atmosphere of southern China during autumn.

The second coastal site, Wenling (WL_c; 28.40 ° N， 121.61 ° E), was situated in a flat ground area in a peninsula in the southeast of China, surrounding by only farmland. The sampling inlet was about 4 m above the ground level. The East China Sea was up to 2 km away from the site to the northeast and southeast. The city of Taizhou was about 30 km away to the northwest of the site. Wind direction ranged from north to east during

the whole campaign at WL_c site, resulting in a variety of air masses that can be encountered from modified clean maritime air mass to polluted continental air mass.

The third coastal site, Changdao (CD_c; 37.99 °N, 120.70 °E), was located at ~50 m above the sea level on a hill in the north coast of an island. This island lied offshore to the east edge of central eastern China and laid between the Jiaodong and the Liaodong Peninsula in the Bohai Sea, called Changdao. The Changdao Island was surrounded by sea on three sides and connected with a larger island by a bridge on the south side. A detailed geographic description of the measurement site is presented in (*Hu et al.*, 2013).

2.1.4 Ship cruise measurement

Ship cruise measurement (ES_s) was carried out on the "Dong Fang Hong 2", which is a multi-functional marine research vessel (http://eweb.ouc.edu.cn/4b/61/c4169a19297/page.htm). The observatory was located on the 6th floor of the "Dong Fang Hong 2", which was about 15 m above the sea level. The vessel sailed from Qingdao of Shandong province (24.5 ℃N, 118.1 ℃E) on March 17th, reached the southernmost area of the cruise near Wenzhou of Zhejiang province on March 27th, and returned at Qingdao (24.5 ℃N, 118.1 ℃E) on April 9th. The study area of the whole cruse covered both the East China Sea and Yellow Sea of China (see Figure 1).

2.2 Instrumentation

The Scanning Mobility Particle Sizer (SMPS, TSI Inc.) system was used to obtain PNDs in the 15-600 nm (mobility diameter) size range at all the 13 sites. The SMPS system includes one Differential Mobility Analyzer (DMA) and one Condensation Particle Counter (CPC). The time resolution of this system was 5 min and the flow rates of sample and sheath air were 0.3 and 3.0 L/min, respectively. The relative humidity of sample air was kept below 40% by a silica diffusion dryer within the inlet lines and sheath air cycles. Size-dependent particle losses inside the instruments as well as in the sampling tubes are calculated (*Willeke*, 1993), and the data are corrected by the obtained correction parameters for each site.

2.3 Parameterization

PNDs at each site are parameterized by a multiple log-normal distribution function. Each mode is described by the following function (*Seinfeld and Pandis, 1998*):

$$\frac{dN_i}{dlogD_p} = \frac{N_i}{\sqrt{2\pi}logσ_i}\exp\left[-\frac{\left(logD_p - logμ_i\right)^2}{2(logσ_i)^2}\right] \quad (1)$$

Where N_i, μ_i and σ_i are the total number concentration, mean diameter and geometric mean standard deviation of the distribution of mode *i*, respectively. The task of the fitting program is to minimize the residual part Q, which is described as:

$$Q = \int_{15}^{600} \frac{\left|dN/dlogD_p - \sum_i dN_i/dlogD_p\right|}{dN/dlogD_p} dlogD_p \quad (2)$$

The growth rate (GR) of newly formed particles and condensational sink (CS) are calculated for NPF events. The CS determines the how quickly of the gaseous molecules can condense onto the pre-existing aerosols and can be calculated by using Equation (3) (*Kulmala et al., 2001, 2012*).

$$CS = 2\pi D\int_{15}^{600} D_p\beta_M\left(D_p\right)n\left(D_p\right)dlogD_p = 2\pi D\sum_i \beta_M D_{p,i}N_i \quad (3)$$

Here D is the diffusion coefficient; n(D_p) represents the dry particle size distribution function; β_M is the transitional correction factor for the mass flux; and N_i is the particle number concentration in the size section *i*. The CS value in NPF days is calculated as the mean value between 9:00 to 12:00 h (local time) of the day. It should be noted that the CS values calculated here are based on the dry particle number size distributions, which may underestimate the real CS values in ambient humidity.

GR is calculated using the Equation (4) (*Kulmala et al.*, 2012):

$$GR = \frac{\Delta D_{p,m}}{\Delta t} \quad (4)$$

Where $D_{p,m}$ is a mean geometric diameter resulted from the log-normal fitting of the particle number size distribution. The methods for calculating both CS and GR are described by Wu et al. (2007).

The critical diameter ($D_{p,crit}$) at which 50% of the particles are activated at the super saturation (S_c) can be calculated based on the knowledge of ambient Kappa (κ) value expressed by Eq. (5) (*Petters and Kreidenweis*, 2007).

$$\kappa = \frac{4A^3}{27D_{Pcrit}^3 ln^2 S_c} \quad (5)$$

$$A = \frac{4\sigma_{s/a} M_w}{RT\rho_w} \quad (6)$$

Where κ is the hygroscopicity parameter used to model the composition-dependence of the solution water activity; $\sigma_{s/a}$ is the droplet surface tension (assumed to be that of pure water with a value of 0.0728 N m^{-2}); M_w is the molecular weight of water; ρ_w is the density of liquid water (g cm^{-3}); R is the universal gas constant (J $mol^{-1}K^{-1}$), and T is the absolute temperature (K).

3 Results and discussion

3.1 Spatial and seasonal variability of PND

The statistics of PNC in the 15-600 nm size range are given in Table 2. Average and median PNCs at all sites were in the range of 0.5-2.8 $\times 10^4$ cm^{-3} and 0.4-2.2 $\times 10^4$ cm^{-3}, respectively. The median PNC at urban (1.1-2.2 $\times 10^4$ cm^{-3}) and regional sites (0.8-1.5 $\times 10^4$ cm^{-3}) were two-times larger than those at coastal/background (0.4-0.6 $\times 10^4$ cm^{-3}) and cruise measurement (0.5 $\times 10^4$ cm^{-3}). The highest PNCs were observed at UR_u site due to frequent NPF events, as well as intensive primary emissions, such as coal combustions for local industries, heating supply and residents' use (*Li et al.*, 2008). The average observed PNCs at Chinese urban sites (1.8 $\times 10^4$ cm^{-3}) were higher than those in European cities which were reported as 1.6-7.0 $\times 10^3$ cm^{-3} and 1.6±0.8 $\times 10^4$ cm^{-3} by *Borsos et al.* (2012) and *Kumar et al.* (2013a), respectively, suggesting a much larger

exposure risks to Chinese population compared with those in European cities. Meanwhile, the average PNCs in low aerosol-loading area (coastal/background sites) in China were still two-fold higher than those in European countries (*Asmi, A. et al.*, 2011). This suggests that the high aerosol loading in the background areas of China increases the background aerosol concentration.

Peak diameters for measured size distributions are calculated in the range of 24-123 nm at all sites (Table 2). The peak diameters were found higher at regional sites (89 nm on average) than at urban sites (69 nm on average). Aging of particles during their transport from urban to regional area likely leads to the growth of particle diameters (*Moffet and Prather*, 2009), which leads to the largest particle peak diameters at regional sites despite the frequent NPF events at these sites. Besides, particle emissions from biomass burning in regional areas have diameter larger than 100 nm (*Reid et al.*, 2005), and may influence the diameter of ambient particles at regional sites. At coastal sites, the peaks of particle size distributions were not as sharp as those seen at other sites (Fig. 2). The PNCs show a wide variation near the peak diameters, as both clean background episodes and polluted episodes caused by transportation occurred in these areas (*Hu et al.*, 2013).

The median particle size distribution at most of the sites can be fitted into three modes. The peak diameters of these modes were in the range of 132-327 nm for the first mode (which can be roughly recognized as accumulation mode), 59-116 nm for the second mode (which can be roughly recognized as Aitken mode), and 17-38 nm for the third mode (which can be roughly recognized as nucleation mode or the second Aitken mode) (Table 2). At HS_r, CD_r and ES_s sites, the fitting exercises give only the first and second modes.

Strong seasonal variations were found at JX_u and WX_u sites, where measurements were conducted both in summer and winter. Higher PNCs in nucleation mode and lower PNCs in accumulation mode were observed in summer measurements.

3.2 Particle number concentration in different size ranges

The PNCs in the 15-600 nm range are separated into three different size groups, which are smaller than 25 nm ($N_{15\text{-}25}$), 25-100 nm ($N_{25\text{-}100}$) and 100-600 nm ($N_{100\text{-}600}$). These three size groups are used to represent three modes of nucleation, Aitken, and accumulation, respectively. The number concentration in each mode can be approximated by integrating certain size distribution using the Equation (7):

$$N_{a-b}(t) = \int_a^b n(D_p, t) d\log D_p = \sum_{i=a}^{b} n_i(D_p, t) \quad (7)$$

Where $N_{a-b}(t)$ represents PNCs in the a-b nm range at a certain time interval, D_p is the geometric mean diameter of the size interval, and n_i is the measured PNC in a particular size interval (cm^{-3}).

As illustrated in Figure 3, the PNCs in each size range show a good log-normal distribution in most cases, but there are still several major differences among the distribution of PNCs in different size ranges at individual sites. The $N_{100\text{-}600}$ at urban and regional sites were much larger than those at coastal sites and cruise measurement, though these values did not show obvious differences between urban and regional sites, indicating the regional feature of secondary aerosols in the whole region of city clusters. Mean $N_{25\text{-}100}$ values appeared to be up to 10-times higher than those in 100-600 nm size range at urban sites, but no significant difference was found at other sites (figure 3), suggesting the emission from road vehicles at urban sites. The distributions of both $N_{15\text{-}25}$ and $N_{25\text{-}100}$ show a very "narrow" distribution at most studying sites compared with European countries (*Asmi, A. et al.*, 2011), mainly because there was seldom clean episodes with very few particles in the atmosphere in China. Even if the air mass was coming from the clean remote continental or oceanic region, the new particle formation and high flux of primary particle emission would increase the $N_{15\text{-}25}$ and $N_{25\text{-}100}$ within a short time (*Wu et al.*, 2008). The PNCs of nucleation mode ($N_{15\text{-}25}$) particles at coastal sites were lower than those of $N_{100\text{-}600}$ and $N_{25\text{-}100}$, especially in autumn and winter, suggesting that either the nucleation rate was low, or high proportion of nucleation mode particles coagulated onto the surfaces of larger particles. Besides, a "wide"

distribution (figure 3c) of N_{15-25} indicates that though the nucleation rate was low most of time at coastal sites, a few NPF events with high concentration in nucleation mode still occurred.

3.3 Diurnal variation of PND

Fig. 4 shows the diurnal variations of the average PND at all the measurement sites. These figures are sorted by seasons and site types. Diurnal PND at nearly all the measurement sites presents a build-up of high concentration belts with peak diameter between 70 and 150 nm. These belts were much more obvious during night time, when there was neither NPF event nor large amount of primary emissions, and should be recognized as the accumulation mode. As smaller particles in nucleation mode and Aitken mode have large diffusion coefficient which provide them a large possibility to coagulate onto the surfaces of larger-sized particles, the residence time for particles in the boundary layer are short (*Davidson and Wu, 1990*). On the other hand, accumulation mode particles had much longer atmospheric life and experienced longer aging process in the atmosphere, resulting in the appearance of this accumulation belt. The higher concentration and larger diameter of particles in this accumulation belts may reflect higher degree of aging of ambient particles. For example, at some sites such as YF_r and KP_r, the peaks of these layers were about 100-120 nm, larger than those at the urban sites of SH_u and WX_u (about 80-90 nm). Besides, particles at all other sites in the three large city groups (see the black circle in Figure 1) had these high concentration belts, suggesting that the regional pollution feature within the whole city group area. In contrast, no such accumulation belt was found at UR_u site, as the PND at UR_u site was largely influenced by the large primary emissions and NPF.

There were large concentrations of nucleation mode particles in the middle of the day at most of studying sites (Figure 4), showing the contribution of the NPF events to the PNC during the whole measurements. The contributions to the PNCs were much more obvious in summer time due to much more NPF events. On the other hand, the PNCs of nucleation mode were pretty low at any time of day during both the winter

measurement campaigns and some of the autumn measurements since there was no NPF event found (Table 3). Compared with urban and regional sites, influence of PNC at coastal/background sites by NPF events was much lower due to the lower concentration of precursor gases (e.g. SO_2) at these sites.

Besides the peak of NPF events around the noon, there were another two concentration peaks during morning (between 07:00 and 09:00 h) and evening (between 17:00 and 20:00 h) rush hours at most of the urban sites, with the size of the peaks about 30-70 nm. The appearance of these peaks was due to the primary emissions from vehicles as well as the diurnal change of the height of boundary layers (*Lin et al.*, 2009). In the meanwhile, at regional sites there were also two concentration peaks at the same time of day. The difference is that at regional sites the sizes of these peaks were much larger (about 70-150 nm) than at urban sites. This reveals the fact that biomass burning in the regional farmland contribute large amount of primary particles (*Huang et al.*, 2011; *Reid et al.*, 2005). Besides, such morning and evening peaks were not found at coastal sites, confirming that there was no primary emission near these coastal sites.

3.4 Frequencies and parameters of NPF events

Obvious NPF events were recognized during most of our measurements. The criterion for discerning NPF events in this study includes three steps. First, there should be a burst of PNC in nucleation mode (below 25 nm in diameter) (*Birmili and Wiedensohler*, 2000). Second, primary emitted species, such as black carbon and CO concentrations should not enhance significantly. Third, the event should last for more than 2 hours, with the increase in particle diameter. As the lower cut-off diameter of our measurements was 15 nm, which is much larger than the size of nucleation clusters (1.5-2 nm) (*Kulmala et al., 2013*), the NPF events might occur 1 to 2 hours before we observed them. Two typical types of NPF events (the “banana” and the “apple”, which were classified by *Wu et al (*2007)) were observed at a number of our sites. The frequencies of NPF events at urban and regional sites (38%) were similar to previous studies that focused on the NPF events in some other sites in China (*Wu et al.*, 2007; *Yue et al.*, 2013) and were much higher than at coastal sites and cruise measurement

(14%) during our measurements (Figure 5).

Sulfuric acid is a well-known precursor for nucleation (*Boy et al.*, 2005; *Zhang*, 2010; *Yue et al.*, 2010; *Andreae*, 2013). High concentrations of SO_2 and OH provide strong source of sulfuric acid at urban and regional sites, and promote the NPF events. On the other hand, the aerosol loading in the ambient atmosphere acts as the condensation and coagulation sink and thus restrains the NPF event. Though the high concentration of pre-existing particles can hinder the NPF in urban and regional areas, there will also be high precursor concentration (such as SO_2, and VOCs) and strong oxidation (performed as high O_3 and OH radical concentration) in these areas, which will favor the NPF. At urban and regional sites in our study, the high precursor concentration and strong oxidation may play a more crucial role than the high concentration of pre-existing particles, leading to the high frequency of NPF events. On the other hand, in the clean coastal area in China, concentrations of precursors as well as the particles are not as high as in urban area as both gases and particles will be dilute during the transport from polluted region to clean coastal area. However, unlike the particles, the gaseous precursors may also undergo continually atmospheric oxidation and transform into particle phase during the transport, which makes the reduction of gaseous precursors larger than the reduction of particles, resulting in fewer NPF events at coastal sites. Besides, other reasons such as meteorological conditions might also affect the frequency of NPF events at diversified sites. In polluted areas, the NPF events are often expected to occur since the air mass is coming from the clean continental background and is not greatly influenced by the polluted urban air (*Wu et al.*, 2007). At coastal sites, however, no NPF events were noted when the air mass was coming from the ocean side with clean air, as this cleaner air mass was not carrying enough NPF precursors such as H_2SO_4 or low-volatile VOCs to favor the nucleation events. This is substantiated by the fact that SO_2 concentrations in the air coming from ocean side were much lower than those coming from the continent (e.g., at BG_c site, average SO_2 concentration in the air mass from ocean and continent were 1.4 ppbv and 2.8 ppbv, respectively) and supported by other studies at coastal site (*Yu et al., 2014*).

The CS values of NPF events are calculated as the mean CS value between 9:00 to 12:00 h (local time) of the day (Eq. 3). In general, CS in all NPF days were in the range of 0.9-5.6 $\times 10^{-2}$ s^{-1} at urban sites, 0.3-8.6 $\times 10^{-2}$ s^{-1} at regional sites, 1.1-2.6 $\times 10^{-2}$ s^{-1} at coastal/background sites and 0.9-1.1 $\times 10^{-2}$ s^{-1} during cruise measurement (see Table 3). The upper limits of CS at urban and regional sites were far larger compared with those at coastal/background sites and cruise measurement and at other sites in western countries (Table 3), which further confirms the fact that NPF events can occur under high aerosol loading in polluted areas in China (*Wu et al.*, 2007). On the other hand, the lower limit of CS at different sites showed no obvious difference, indicating that there are "clean case" NPF events even in these polluted urban areas (*Wu et al.*, 2007).

The GRs of newly formed particles (calculated from 15 nm to 30 nm) ranged from 4.2 to 18.1 nm h^{-1} at urban sites, 3.2 to 21 nm h^{-1} at regional sites, and 1.6 to 7.5 nm h^{-1} at both coastal sites and cruise measurement (Table 3). The highest GR was found at YF_r site (regional) with value of 21 nm h^{-1}. Average GRs at urban and regional sites were about twice those at coastal sites and cruise measurement (Table 3), indicating that the higher concentrations of gaseous precursors in the polluted areas not only favor the formation of particles, but also accelerate the growth rate as long as the nucleation particles are formed.

Both the CS and GR results in our study are comparable to other studies performed in Beijing (*Wu et al.*, 2007), Back-garden (*Yue et al.*, 2013), and Xinken (*Liu et al.*, 2008), in China. CS values in our study are generally higher than those at European and American sites and smaller than those at some sites in developing countries, such as New Delhi (see Table 3). The GR values show no obvious differences between China and other countries (both in developed and developing countries) at the same site types (see Table 3).

3.5 Evaluation of the contribution of NPF to potential CCN

The basic idea to estimate the production of potential CCN from NPF events is based on the assumption that particles larger than a certain diameter could be served as

CCN. As the newly formed particles consist mainly ammonium sulfate and secondary organics (*Yue et al.*, 2010) and primary emission particles contain a lot of black carbon and hydrophobic organics (*Medalia and Rivin*, 1982; *Reid et al.*, 2005), the κ value for newly formed particles and primary emission particles may be of large difference. Some previous studies in China have concluded that the average κ value of all ambient particles is about 0.3 for many environments in China (*Gunthe et al.*, 2011; *Yue et al.*, 2010; *Rose et al.*, 2010), but few has provieded the κ value of newly formed particles in the atmosphere. In this study, the hygroscopicity parameter κ for the newly formed particles is taken as 0.43 at about 100 nm based on the assumption of one third of chemical components of these particles are organics and others were inorganics (*Gunthe et al.*, 2011; *Yue et al.*, 2010). Therefore, the only task left is to achieve the PND of newly formed particles.

In this study, mode fitting method is used to distinguish the newly formed particles from others. Diurnal half-hourly average PND data are used for the log-normal fitting. A total of three (or four) lognormal modes are achieved in the fitness exercise (see Eq. 1) on the PND data. These include up to two NPF modes (with initial diameter about 15-20 nm, which may grow up to 50 nm later), one Aitken mode (40-100 nm) as well as one accumulation mode (100-500 nm). Figure 6 illustrates an example of the mode fitting result at the site of KP_r, which is a typical regional site with high frequency of NPF events. Half-hourly fitting results in the afternoon from 11:00-16:00 h at KP_r site with two NPF modes and two pre-existing modes are shown in Figure 6. At the site of KP_r, NPF events were observed to occur between mainly between 9:00 and 11:00 h every day, resulting in a sharp and narrow nucleation mode peak at about 19 nm at 11:00 h (Figure 6). In the following five hours, the peak diameter of NPF mode gradually grew from 19 to 50 nm, with the concentration of NPF mode decreasing from 7500 to 5000 cm^{-3} at the same time. Furthermore, when the peak diameters of these log-normal distribution NPF modes reached 50 nm, there would be a large amount of particles with diameter exceed 80 nm or even 100 nm. These particles were large enough to possibly act as CCN under a certain S_c. The contribution of NPF to potential CCN production

can then be calculated by integrating the distribution of the NPF mode particle with diameter larger than $D_{p,crit}$. As it is challenging to extract NPF mode when the NPF peaks are submerged in the size distribution of ambient particles, in order to achieve accurate fitness results, prominent NPF peak in the size distribution is required. Therefore, our subsequent discussions are focused on the time period from 13:00 to 17:00 h in the afternoon, as the time is neither too early for the formation of new particles, nor too late for primary emission to perform a dominate role in the ambient PND.

The contributions of NPF and growth to potential CCN concentration in all measurements are calculated through this approach. Results of this exercise are illustrated in Table 4. Two values of super saturations are assumed here as 0.5% and 0.2%, with critical diameter of 50 nm and 91 nm for newly formed particles, and 60 nm and 100 nm for other particles, respectively. Contributions of NPF to potential CCN concentration varied greatly during different measurements, ranging from 0% to 66% when S_c is 0.5, and 0% to 24% when S_c is 0.2 (Table 4). The highest values were found in the summer at WX_u site. During summertime, the average contributions values at urban and regional sites were 50% (S_c = 0.5) and 18% (S_c = 0.2), which were much higher than those in other seasons. The strong oxidation condition in summer favors the formation of new NPF as well as the growth of newly formed particles, accelerating the newly formed particles to perform as CCN. On the contrary, the contribution is 0% during two winter measurements, as no NPF events were observed during these two measurements.

Weighted average contributions for different size types are roughly calculated. Annual average contribution of NPF to CCN at urban, regional and coastal sites were found to be 33%, 19%, 7% (at S_c=0.5), and 11%, 6%, 0% (at S_c=0.2), respectively. Good correlation (R^2=0.7) between growth rate of NPF and contribution to CCN among all sties was found, indicating that growth rates of NPF events are the decisive factor in the conversion of newly formed particle to possible CCN (*Yue et al.*, 2011).

Although there were two NPF events during the cruise measurement, no

contribution to CCN concentration was found by any of these NPF events, because the diameter of these secondary particles did not meet the critical diameter for CCN. *Zhang et al.* (2012) demonstrated that NPF in marine environment is not likely to produce particles of the size of CCN. Our study further confirms that the NPF events show little impact on the concentration of CCN in the marine area near polluted continent. It may need more than one day for the newly formed particles to perform as CCN.

In previous studies, people always use the CCN concentration enhancement factor to describe the contribution of NPF events to corresponding CCN (*Yue et al., 2011*; *Kuang et al.*, 2009; *Lihavainen et al.*, 2003). It is obtained by dividing the concentration of CCN-sized particles after a NPF event by that prior to the event. The average CCN enhancement factors after the NPF events at $S_c = 0.2$ ($D_{p,crit} = 100$ nm) were calculated to be 1.5 at a remote site in Northern Finland (*Lihavainen et al.*, 2003) and in the range of 1.5-2.5 in Beijing (*Yue et al.*, 2011). Similar conclusion was obtained in Botsalano, but with great seasonal variation (*Laakso et al.*, 2013). The factors in these studies are higher than in our study because they only considered NPF days. The values would be much lower and similar to our result if the enhancements were multiplied by the frequencies of NPF events. Besides, the method used in these studies did not consider the influence of primary emissions and change of boundary layer height on CCN concentration (*Laakso et al.*, 2013) and thus may overestimate the enhancements. In our study, all the sites were away from main road and stationary sources, PNCs of primary emission were not expected to change much during the focused time intervals. Besides, the mode fit method has considered the non-NPF particles. Therefore, our results are not influenced greatly by the primary emissions. However, the approach to calculate the contribution of NPF to CCN also has some uncertainties and limitations. First, we can only calculate the contribution to CCN production by the NPF event in the same day. Some of the pre-existing particles before NPF events may also come from the NPF in previous days, but these can only be recognized as pre-existing particles rather than NPF particles through our approach. This is likely to result in underestimation of the contribution. Second, even though our method has its advantage

on distinguish the nucleation particles from non-NPF particles, some non-NPF particles may have a chance to be recognized as nucleation particle when we perform the processing of diurnal average PNCs, which may lead to overestimation of results. Third, as discussed above, the approach requires very clear NPF peaks in the size distributions in order to achieve accurate fitness results. So the focusing time period is constrained between 14:00 and 17:00 h, when the NPF mode is clear and evening rush hour has not come. The contribution in the following hours or the following days cannot be precisely calculated though this approach. As it is crucial to evaluate the contribution of NPF events to CCN production in the following days, more studies on this field are needed in the future. Nevertheless, based on field measurements, our work provides annual and seasonal average contribution of NPF events to CCN production for the first time in diversified Chinese atmosphere. The estimation of contribution of NPF events to corresponding CCN might be particularly useful for the validation of global climate models.

4. Summary and conclusions

This paper presents size-resolved measurements of submicron aerosol in the 15-600 nm size range during the 15 individual field campaigns, taken between 2008 and 2011, at thirteen different sites in China. These sites include 5 urban sites, 4 regional sites, 3 coastal/background sites and one ship cruise measurement, and are mainly located within the three largest city clusters of China.

The particle number size distributions were fitted into three modes (nucleation, Aitken, accumulation) at most of the sites. The median PNC at urban (1.1-2.2 $\times 10^4$ cm^{-3}) and regional sites (0.8-1.5 $\times 10^4$ cm^{-3}) are two-times larger than those at coastal and background (0.4 -0.6 $\times 10^4$ cm^{-3}) sites and cruise measurement (0.5 $\times 10^4$ cm^{-3}).

Primary emission from road vehicles as well as regional biomass burning appears to have a large contribution to the ambient PNCs. High emissions from road vehicles at urban sites resulted in up to 10-times higher $N_{25\text{-}100}$ than those of $N_{100\text{-}600}$. PNCs in both size ranges were nearly identical at all other sites. Vehicular emissions at urban sites

and biomass burning emission at regional sites led to two concentration peaks in the early morning and evening hours.

Regional secondary aerosol pollution is a main feature for the submicron aerosol pollution in China. No obvious differences in the $N_{100\text{-}600}$ particles were observed between urban and regional sites. Diurnal variations show a build-up of high concentration accumulation belt at all the regional sites.

The occurrence frequencies of the NPF events in high aerosol-loading environment of China were found to be higher than those in less aerosol-loading environments. High gaseous precursors and strong oxidation at urban and regional sites not only favor the formation of particles, but also accelerate the growth rate after the nucleation mode particles are formed. The average GR of nucleation mode particles were 8.0-10.9 nm h^{-1} at urban sites, 7.4-13.6 nm h^{-1} at regional sites and 2.8-7.5 nm h^{-1} at coastal sites and cruise measurement. The NPF events in the less aerosol-loading environment were found to be greatly influenced by pollutant transport.

Average contributions of NPF events to potential CCN are calculated in this study. Contributions of NPF events to potential CCN at 0.2 super-saturation in the afternoon of all measurement days were 11% and 6% at urban sites and regional sites, respectively. On the other hand, NPF events at coastal sites and cruise measurement had little impact on potential CCN.

Our study presents a unique dataset of aerosol size distributions and general concepts of the features of submicron particle pollution along with the fundamental drivers of particulate pollution in China. Besides, our estimation of contribution of NPF events to corresponding CCN might be particularly useful for the validation of global climate models.

5. Acknowledgement

This work was supported by the National Natural Science Foundation of China (21025728 and 21190052), the National Basic Research Program of

China (2013CB228503) and the China Ministry of Environmental Protection's Special Funds for Scientific Research on Public Welfare (201009002). Prashant Kumar, Jianfei Peng and Min Hu thank the University of Surrey's International Relations Office for the Santander Postgraduate Mobility Award that helped Jianfei Peng to visit University of Surrey, UK, to develop this research article collaboratively.

References

Andreae, M. O.: The Aerosol Nucleation Puzzle, Science, 339, 911-912, doi:10.1126/science.1233798, 2013.

Asmi, A., Wiedensohler, A., Laj, P., Fjaeraa, A. M., Sellegri, K., Birmili, W., Weingartner, E., Baltensperger, U., Zdimal, V., Zikova, N., Putaud, J. P., Marinoni, A., Tunved, P., Hansson, H. C., Fiebig, M., Kivekäs, N., Lihavainen, H., Asmi, E., Ulevicius, V., Aalto, P. P., Swietlicki, E., Kristensson, A., Mihalopoulos, N., Kalivitis, N., Kalapov, I., Kiss, G., de Leeuw, G., Henzing, B., Harrison, R. M., Beddows, D., O'Dowd, C., Jennings, S. G., Flentje, H., Weinhold, K., Meinhardt, F., Ries, L., Kulmala, M.: Number size distributions and seasonality of submicron particles in Europe 2008–2009, Atmospheric Chemistry and Physics, 11, 5505-5538, doi:10.5194/acp-11-5505-2011, 2011.

Asmi, E., Kivekas, N., Kerminen, V. M., Komppula, M., Hyvarinen, A. P., Hatakka, J., Viisanen, Y., and Lihavainen, H.: Secondary new particle formation in Northern Finland Pallas site between the years 2000 and 2010, Atmospheric Chemistry and Physics, 11, 12959-12972, 2011.

Bigi, A., and Ghermandi, G.: Particle Number Size Distribution and Weight Concentration of Background Urban Aerosol in a Po Valley Site, Water, Air, & Soil Pollution, 220, 265-278, doi:10.1007/s11270-011-0752-6, 2011.

Borsos, T., Rimnacova, D., Zdimal, V., Smolik, J., Wagner, Z., Weidinger, T., Burkart, J., Steiner, G., Reischl, G., Hitzenberger, R., Schwarz, J., and Salma, I.: Comparison of particulate number concentrations in three Central European capital cities, Science Total Environment, 433, 418-426, 2012.

Boy, M., Kulmala, M., Ruuskanen, T. M., Pihlatie, M., Reissell, A., Aalto, P. P., Keronen, P., Dal Maso, M., Hellen, H., Hakola, H., Jansson, R., Hanke, M., and Arnold, F.: Sulphuric acid closure and contribution to nucleation mode particle growth. Atmospheric Chemistry and Physics, 5, 863-878, 2005.

Buseck, P. R., and Adachi, K.: Nanoparticles in the Atmosphere, Elements, 4, 389-394, doi:10.2113/gselements.4.6.389, 2008.

Creamean, J. M., Ault, A. P., Ten Hoeve, J. E., Jacobson, M. Z., Roberts, G. C., and Prather, K. A.: Measurements of Aerosol Chemistry during New Particle Formation Events at a Remote Rural Mountain Site, Environmental Science & Technology, 45, 8208-8216, 2011.

Dal Maso, M., Kulmala, M., Riipinen, I., Wagner, R., Hussein, T., Aalto, P. P., and Lehtinen, K. E. J.: Formation and growth of fresh atmospheric aerosols: eight years of aerosol size distribution data from SMEAR II, Hyytiala, Finland, Boreal Environment Research, 10, 323-336, 2005.

Davidson, C. I., and Wu, Y. L.: Dry deposition of particles and vapors, in Acid Precipitation, Vol. 3, S. E. Lindberg, A. L. Page, and S. A. Norton, eds., Springer-Verlag, Berlin, pp. 103-209, 1990.

Du, J. F., Cheng, T. T., Zhang, M., Chen, J. M., He, Q. S., Wang, X. M., Zhang, R. J., Tao, J., Huang, G. H., Li, X., and Zha, S. P.: Aerosol Size Spectra and Particle Formation Events at Urban Shanghai in Eastern China, Aerosol Air Qual Res, 12(6), 1362-1372, 2012.

Dunn, M. J., Jimenez, J. L., Baumgardner, D., Castro, T., McMurry, P. H., and Smith, J. N.: Measurements of Mexico City nanoparticle size distributions: Observations of new particle formation and growth, Geophys. Res. Lett., 31, L10102, doi:10.1029/2004GL019483, 2004.

Dusek, U., Frank, G. P., Hildebrandt, L., Curtius, J., Schneider, J., Walter, S., Chand, D., Drewnick, F., Hings, S., Jung, D., Borrmann, S., and Andreae, M. O.: Size Matters More Than Chemistry for Cloud-Nucleating Ability of Aerosol Particles, Science, 312, 1375-1378, doi:10.1126/science.1125261, 2006.

Gao, J., Chai, F. H., Wang, T., and Wang, W. X.: Particle number size distribution and new particle formation (NPF) in Lanzhou, Western China, Particuology, 9, 611-618, 2011.

Gong, Z. H., Lan, Z. J., Xue, L., Zeng, L. W., He, L. Y., and Huang, X. F.: Characterization of submicron aerosols in the urban outflow of the central Pearl River Delta region of China, Frontiers of Environmental Science & Engineering, 6, 725-733, 2012.

Gunthe, S. S., Rose, D., Su, H., Garland, R. M., Achtert, P., Nowak, A., Wiedensohler, A., Kuwata, M., Takegawa, N., Kondo, Y., Hu, M., Shao, M., Zhu, T., Andreae, M. O., and Pöschl, U.: Cloud condensation nuclei (CCN) from fresh and aged air pollution in the megacity region of Beijing, Atmospheric Chemistry and Physics, 11, 11023-11039, doi:10.5194/acp-11-11023-2011, 2011.

Guo, S., Hu, M., Wang, Z. B., Slanina, J., and Zhao, Y. L.: Size-resolved aerosol water-soluble ionic compositions in the summer of Beijing: implication of regional secondary formation, Atmospheric Chemistry and Physics, 10, 947-959, 2010.

Hamed, A., Joutsensaari, J., Mikkonen, S., Sogacheva, L., Dal Maso, M., Kulmala, M., Cavalli, F., Fuzzi, S., Facchini, M. C., Decesari, S., Mircea, M., Lehtinen, K. E. J., and Laaksonen, A.: Nucleation and growth of new particles in Po Valley, Italy, Atmospheric Chemistry and Physics, 7, 355-376, 2007.

Harrison, R. M., Beddows, D. C. S., and Dall'Osto, M.: PMF Analysis of Wide-Range Particle Size Spectra Collected on a Major Highway, Environmental Science & Technology, 45, 5522-5528 2011.

Heal, M. R., Kumar, P., and Harrison, R. M.: Particles, air quality, policy and health, Chemical Society Reviews, 41, 6606-6630, 2012.

Herrmann, E., Ding, A. J., Kerminen, V. M., Petaja, T., Yang, X. Q., Sun, J. N., Qi, X.

M., Manninen, H., Hakala, J., Nieminen, T., Aalto, P. P., Kulmala, M., Fu, C. B.: Aerosols and nucleation in eastern China: first insights from the new SORPES-NJU station, Atmospheric Chemistry and Physics, 4, 2169-2183, 2014.

Hu, W. W., Hu, M., Yuan, B., Jimenez, J. L., Tang, Q., Peng, J. F., Hu, W., Shao, M., Wang, M., Zeng, L. M., Wu, Y. S., Gong, Z. H., Huang, X. F., and He, L. Y.: Insights on organic aerosol aging and the influence of coal combustion at a regional receptor site of central eastern China, Atmospheric Chemistry and Physics, 13, 10095-10112, doi:10.5194/acp-13-10095-2013, 2013.

Huang, X. F., He, L. Y., Hu, M., Canagaratna, M. R., Kroll, J. H., Ng, N. L., Zhang, Y. H., Lin, Y., Xue, L., Sun, T. L., Liu, X. G., Shao, M., Jayne, J. T., and Worsnop, D. R.: Characterization of submicron aerosols at a rural site in Pearl River Delta of China using an Aerodyne High-Resolution Aerosol Mass Spectrometer, Atmospheric Chemistry and Physics, 11, 1865-1877, 2011.

Huang, X. F., He, L. Y., Xue, L., Sun, T. L., Zeng, L. W., Gong, Z. H., Hu, M., and and Zhu, T.: Highly time-resolved chemical characterization of atmospheric fine particles during 2010 Shanghai World Expo, Atmospheric Chemistry and Physics, 12, 4897-4907, 2012.

Iida, K., Stolzenburg, M. R., McMurry, P. H., and Smith, J. N.: Estimating nanoparticle growth rates from size-dependent charged fractions: Analysis of new particle formation events in Mexico City, Journal of Geophysical Research-Atmospheres, 113, D05207 doi: 10.1029/2007JD009260, 2008.

IPCC (Intergovernmental Panel on Climate Change): Climate Change 2007: The Physical Science Basis. Contribution of Working Group I to the Fourth Assessment, Report of the Intergovernmental Panel on Climate Change, Cambridge University Press, Cambridge, United Kingdom, and New York, NY, USA..

Kerminen, V. M., Paramonov, M., Anttila, T., Riipinen, I., Fountoukis, C., Korhonen, H., Asmi, E., Laakso, L., Lihavainen, H., Swietlicki, E., Svenningsson, B., Asmi, A., Pandis, S. N., Kulmala, M., and Petaja, T.: Cloud condensation nuclei production associated with atmospheric nucleation: a synthesis based on existing literature and new results, Atmospheric Chemistry and Physics, 12, 12037-12059, 2012.

Kuang, C., McMurry, P. H., and McCormick, A. V.: Determination of cloud condensation nuclei production from measured new particle formation events, Geophysical Research Letters, 36, L09822, doi:10.1029/2009GL037584, 2009.

Kulmala, M., Dal Maso, M., Makela, J. M., Pirjola, L., Vakeva, M., Aalto, P., Miikkulainen, P., Hameri, K., O'Dowd, C. D.: On the formation, growth and composition of nucleation mode particles. Tellus B, 53, 479-490, 2001.

Kulmala, M., Kontkanen, J., Junninen, H., Lehtipalo, K., Manninen, H. E., Nieminen, T., Petaja, T., Sipila, M., Schobesberger, S., Rantala, P., Franchin, A., Jokinen, T., Jarvinen, E., Aijala, M., Kangasluoma, J., Hakala, J., Aalto, P. P., Paasonen, P., Mikkila, J., Vanhanen, J., Aalto, J., Hakola, H., Makkonen, U., Ruuskanen, T., Mauldin, R. L., Duplissy, J., Vehkamaki, H., Back, J., Kortelainen, A., Riipinen, I., Kurten, T., Johnston, M. V., Smith, J. N., Ehn, M., Mentel, T. F., Lehtinen, K. E. J., Laaksonen, A., Kerminen, V. M., Worsnop, D. R..: Direct observations of

atmospheric aerosol nucleation, Science, 339, 943-946, doi:10.1126/science.1227385, 2013.
Kulmala, M., Petaja, T., Nieminen, T., Sipila, M., Manninen, H. E., Lehtipalo, K., Dal Maso, M., Aalto, P. P., Junninen, H., Paasonen, P., Riipinen, I., Lehtinen, K. E. J., Laaksonen, A., Kerminen, V. M.: Measurement of the nucleation of atmospheric aerosol particles, Nature Protocols 7,1651-1667, 2012.
Kumar, P., Morawska, L., Birmili, W., Paasonen, P., Hu, M., Kulmala, M., Harrison, R. M., Norford, L., and Britter, R.: Ultrafine particles in cities, Environment International, 66, 1-10, 2014.
Kumar, P., Morawska, L., and Harrison, R. M.: Nanoparticles in European cities and associated health impacts. In Urban Air Quality in Europe: The Handbook of Environmental Chemistry (Editor Viana, M.). Springer Berlin Heidelberg, Volume 26, pp. 339-365, http://dx.doi.org/10.1007/698_2012_161, 2013a.
Kumar, P., Pirjola, L., Ketzel, M., and Harrison, R. M.: Nanoparticle emissions from 11 non-vehicle exhaust sources - A review, Atmospheric Environment, 67, 252-277, 2013b.
Kumar, P., Robins, A., Vardoulakis, S., and Britter, R.: A review of the characteristics of nanoparticles in the urban atmosphere and the prospects for developing regulatory controls, Atmospheric Environment, 44, 5035-5052, 2010.
Kumar, P., Gurjar, B.R., Nagpure, A., and Harrison, R. H.: Preliminary estimates of particle number emissions from road vehicles in megacity Delhi and associated health impacts. Environmental Science and Technology, 45, 5514-5521, 2011.
Laakso, L., Merikanto, J., Vakkari, V., Laakso, H., Kulmala, M., Molefe, M., Kgabi, N., Mabaso, D., Carslaw, K. S., Spracklen, D. V., Lee, L. A., Reddington, C. L., and Kerminen, V. M.: Boundary layer nucleation as a source of new CCN in savannah environment, Atmospheric Chemistry and Physics, 13, 1957-1972, doi:10.5194/acp-13-1957-2013, 2013.
Li, J., Zhuang, G. S., Huang, K., Lin, Y. F., Xu, C., and Yu, S. L.: Characteristics and sources of air-borne particulate in Urumqi, China, the upstream area of Asia dust, Atmospheric Environment, 42, 776–787, 2008.
Lihavainen, H., Kerminen, V. M., Komppula, M., Hatakka, J., Aaltonen, V., Kulmala, M., and Viisanen, Y.: Production of "potential" cloud condensation nuclei associated with atmospheric new-particle formation in northern Finland, Journal of Geophysical Research-Atmospheres, 108, 4782, doi:10.1029/2003jd003887, 2003.
Lin, M., Holloway, T., Oki, T., Streets, D. G., and Richter, A.: Multi-scale model analysis of boundary layer ozone over East Asia, Atmospheric Chemistry and Physics, 9, 3277-3301, 2009.
Lin, P., Hu, M., Wu, Z., Niu, Y., and Zhu, T.: Marine aerosol size distributions in the springtime over China adjacent seas, Atmospheric Environment, 41, 6784-6796, 2007.
Liu, S., Hu, M., Wu, Z. J., Wehner, B., Wiedensohler, A., and Cheng, Y. F.: Aerosol number size distribution and new particle formation at a rural/coastal site in Pearl River Delta (PRD) of China, Atmospheric Environment, 42, 6275-6283, 2008.
Medalia, A. I., and Rivin, D.: Particulate carbon and other components of soot and

751 carbon-black, Carbon, 20, 481-492, doi:10.1016/0008-6223(82)90084-7, 1982.
752 Merikanto, J., Spracklen, D. V., Mann, G. W., Pickering, S. J., and Carslaw, K. S.:
753 Impact of nucleation on global CCN, Atmospheric Chemistry and Physics, 9, 8601-
754 8616, 2009.
755 Moffet, R. C., and Prather, K. A.: In-situ measurements of the mixing state and optical
756 properties of soot with implications for radiative forcing estimates, Proceedings of
757 the National Academy of Sciences, 106, 11872-11877, 2009.
758 Monkkonen, P., Koponen, I. K., Lehtinen, K. E. J., Hameri, K., Uma, R., and Kulmala,
759 M.: Measurements in a highly polluted Asian mega city: observations of aerosol
760 number size distribution, modal parameters and nucleation events, Atmospheric
761 Chemistry and Physics, 5, 57-66, 2005.
762 Nel, A., Xia, T., Madler, L., and Li, N.: Toxic potential of materials at the nanolevel,
763 Science, 311, 622-627, 2006.
764 Petters, M. D., and Kreidenweis, S. M.: A single parameter representation of
765 hygroscopic growth and cloud condensation nucleus activity, Atmospheric
766 Chemistry and Physics, 7, 1961-1971, 2007.
767 Reid, J. S., Koppmann, R., Eck, T. F., and Eleuterio, D. P.: A review of biomass burning
768 emissions part II: intensive physical properties of biomass burning particles,
769 Atmospheric Chemistry and Physics, 5, 799-825, 2005.
770 Salma, I., Borsos, T., Weidinger, T., Aalto, P., Hussein, T., Dal Maso, M., and Kulmala,
771 M.: Production, growth and properties of ultrafine atmospheric aerosol particles in
772 an urban environment, Atmospheric Chemistry and Physics, 13, 1339-1353, 2011.
773 See, S. W., Balasubramanian, R., and Wang, W.: A study of the physical, chemical, and
774 optical properties of ambient aerosol particles in Southeast Asia during hazy and
775 nonhazy days, Journal of Geophysical Research-Atmospheres, 111, D10S08,
776 doi:10.1029/2005jd006180, 2006.
777 Seinfeld, J. H., and Pandis, S. N.: Atmospheric chemistry and physics. From air
778 pollution to climate change, John Wiley & Sons New York, 429-443, 1998.
779 Shen, X. J., Sun, J. Y., Zhang, Y. M., Wehner, B., Nowak, A., Tuch, T., Zhang, X. C.,
780 Wang, T. T., Zhou, H. G., Zhang, X. L., Dong, F., Birmili, W., and Wiedensohler,
781 A.: First long-term study of particle number size distributions and new particle
782 formation events of regional aerosol in the North China Plain, Atmospheric
783 Chemistry and Physics, 11, 1565-1580, doi:10.5194/acp-11-1565-2011, 2011.
784 Reid, J. S., Eck, T. F., Christopher, S. A., Koppmann, R., Dubovik, O., Eleuterio, D. P.,
785 Holben, B. N., Reid, E. A., and Zhang, J.: A review of biomass burning emissions
786 part III: intensive optical properties of biomass burning particles, Atmospheric
787 Chemistry and Physics, 5, 827-849, 2005.
788 Rose, D., Nowak, A., Achtert, P., Wiedensohler, A., Hu, M., Shao, M., Zhang, Y.,
789 Andreae, M. O., and Poschl, U.: Cloud condensation nuclei in polluted air and
790 biomass burning smoke near the mega-city Guangzhou, China - Part 1: Size-
791 resolved measurements and implications for the modeling of aerosol particle
792 hygroscopicity and CCN activity, Atmospheric Chemistry and Physics, 10, 3365-
793 3383, 2010.
794 Wang, Z. B., Hu, M., Sun, J. Y., Wu, Z. J., Yue, D. L., Shen, X. J., Zhang, Y. M., Pei,

X. Y., Cheng, Y. F., and Wiedensohler, A.: Characteristics of regional new particle formation in urban and regional background environments in the North China Plain, Atmospheric Chemistry and Physics, 13, 12495-12506, 10.5194/acp-13-12495-2013, 2013a.

Wang, Z. B., Hu, M., Wu, Z. J., and Yue, D. L.: Research on the Formation Mechanisms of New Particles in the Atmosphere, Acta Chim. Sin., 71, 519-527, 10.6023/a12121062, 2013b.

Wang, Z. B., Hu, M., Yue, D. L., He, L. Y., Huang, X. F., Yang, Q., Zheng, J., Zhang, R. Y., and Zhang, Y. H.: New particle formation in the presence of a strong biomass burning episode at a downwind rural site in PRD, China, Tellus B, 65, 19965, http://dx.doi.org/10.3402/tellusb.v65i0.19965, 2013c.

Wehner, B., and Wiedensohler, A.: Long term measurements of submicrometer urban aerosols: statistical analysis for correlations with meteorological conditions and trace gases, Atmospheric Chemistry and Physics, 3, 867-879, 2003.

Wehner, B., Wiedensohler, A., Tuch, T. M., Wu, Z. J., Hu, M., Slanina, J., and Kiang, C. S.: Variability of the aerosol number size distribution in Beijing, China: New particle formation, dust storms, and high continental background, Geophysical Research Letters, 31, L22108, DOI: 10.1029/2004GL021596, 2004.

WHO: Review 5 of evidence on health aspects of air pollution – REVIHAAP. World Health Organisation, Regional Office for Europe, available at: http://www.euro.who.int/__data/assets/pdf_file/0020/182432/e96762-final.pdf (last access: 5 June 2014), 2013.

Wiedensohler, A., Cheng, Y. F., Nowak, A., Wehner, B., Achtert, P., Berghof, M., Birmili, W., Wu, Z. J., Hu, M., Zhu, T., Takegawa, N., Kita, K., Kondo, Y., Lou, S. R., Hofzumahaus, A., Holland, F., Wahner, A., Gunthe, S. S., Rose, D., Su, H., and Poschl, U.: Rapid aerosol particle growth and increase of cloud condensation nucleus activity by secondary aerosol formation and condensation: A case study for regional air pollution in northeastern China, Journal of Geophysical Research-Atmospheres, 114, D00G08, DOI: 10.1029/2008JD010884, 2009.

Willeke, K. and Baron, P. A.: Aerosol Measurement Principles, Techniques, and Applications, Van Nostrand Reinhold, Hoboken, NJ, 1993.

Wu, Z.J., Hu, M., Lin, P., Liu, S., Wehner, B., and Wiedensohler, A.: Particle number size distribution in the urban atmosphere of Beijing, China, Atmos. Environ., 42, 7967-7980, 2008.

Wu, Z. J., Hu, M., Liu, S., Wehner, B., Bauer, S., Ssling, A. M., Wiedensohler, A., Petaja, T., Dal Maso, M., and Kulmala, M.: New particle formation in Beijing, China: Statistical analysis of a 1-year data set, Journal of Geophysical Research-Atmospheres, 112, D09209, DOI: 10.1029/2006JD007406, 2007.

Xu, P., Chen, Y. F., and Ye, X. J.: Haze, air pollution, and health in China, Lancet, 382, 2067-2067, 2013.

Yli-Juuti, T., Riipinen, I., Aalto, P. P., Nieminen, T., Maenhaut, W., Janssens, I. A., Claeys, M., Salma, I., Ocskay, R., Hoffer, A., Imre, K., and Kulmala, M.: Characteristics of new particle formation events and cluster ions at K-puszta, Hungary, Boreal Environment Research, 14, 683-698, 2009.

Yu, F., Luo, G., Liu, X., Easter, R. C., Ma, X., and Ghan, S. J.: Indirect radiative forcing by ion-mediated nucleation of aerosol, Atmospheric Chemistry and Physics, 12, 11451-11463, 2012.

Yu, H., Hallar, A.G., You, Y., Sedlacek, A., Springston, S., Kanawade, V.P., Lee, Y.N., Wang, J., Kuang, C.G., McGraw, R.L., McCubbin, I., Mikkila, J., Lee, S.H.: Sub-3nm particles observed at the coastal and continental sites in the United States, Journal of Geophysical Research-Atmospheres, 119, 860-879, 2014.

Yue, D. L., Hu, M., Wang, Z. B., Wen, M. T., Guo, S., Zhong, L. J., Wiedensohler, A., and Zhang, Y. H.: Comparison of particle number size distributions and new particle formation between the urban and rural sites in the PRD region, China, Atmospheric Environment, 76, 181-188, 2013.

Yue, D. L., Hu, M., Zhang, R. Y., Wu, Z. J., Su, H., Wang, Z. B., Peng, J. F., He, L. Y., Huang, X. F., Gong, Y. G., and Wiedensohler, A.: Potential contribution of new particle formation to cloud condensation nuclei in Beijing, Atmospheric Environment, 45, 6070-6077, 2011.

Yue, D. L., Hu, M., Zhang, R. Y., Wang, Z. B., Zheng, J., Wu, Z. J., Wiedensohler, A., He, L. Y., Huang, X. F., and Zhu, T.: The roles of sulfuric acid in new particle formation and growth in the mega-city of Beijing, Atmospheric Chemistry and Physics, 10, 4953-4960, 2010.

Zhang, R. Y.: Getting to the Critical Nucleus of Aerosol Formation, Science, 328, 1366-1367, 2010.

Zhang, R. Y., Khalizov, A., Wang, L., Hu, M., and Xu, W.: Nucleation and Growth of Nanoparticles in the Atmosphere, Chemical Reviews, 112, 1957-2011, 2012.

Zhang, Y. H., Hu, M., Zhong, L. J., Wiedensohler, A., Liu, S. C., Andreae, M. O., Wang, W., and Fan, S. J.: Regional Integrated Experiments on Air Quality over Pearl River Delta 2004 (PRIDE-PRD2004): Overview, Atmospheric Environment, 42, 6157-6173, 2008.

866 **Table 1.** Summary of information providing description of sampling periods at each
867 measurement site. Please note that the words in parenthesis against each site represent
868 a short name of each site, and subscripts u, r, c and s indicate urban, regional, coastal
869 /background and cruise site types, respectively.

Type	Sites	Coordinates	Sampling period	Valid data
Urban	Guangzhou (GZ_u)	23.13˚ N, 113.26˚ E	Nov.12-29, 2010	4766
	Shanghai (SH_u)	31.23˚ N, 21.53˚ E	Apr.15-Jun.22, 2010	18658
	Urumchi (UC_u)	87.58˚ N, 43.83˚ E	May 16-Jun.2, 2008	4835
	Wuxi (WX_u)	31.56˚ N, 120.29˚ E	Jul.21-Aug.7, 2010	4769
			Jan.1-Jan.14, 2011	4926
	Jinhua (JH_u)	29.1 ºN, 119.69 ºE	Oct.29-Nov.28, 2011	7776
Regional	Heshan (HS_r)	22.71 °N, 112.93 °E	Nov.12-29, 2010	4921
	Kaiping (KP_r)	22.33 °N, 112.54 °E	Oct.18-Nov.17, 2008	8465
	Jiaxing (JX_r)	30.8 °N, 120.8 °E	Jun.28-Jul.15, 2010	4564
			Dec.5-22, 2010	4030
	Yufa (YF_r)	39.51 °N, 116.3 °E	Oct.5-31, 2007	5182
Coastal/ Background	Baguang (BG_c)	22.65 °N，114.54 °E	Oct.25-Dec.3, 2009	5895
	Wenling (WL_c)	28.40 °N，121.61 °E	Oct.30-Nov.28, 2011	7064
	Changdao (CD_c)	37.99 °N, 120.70 °E	Mar.19-Apr.24, 2011	10338
Cruise	East China sea (ES_s)	-	Mar.18-Apr.8, 2011	5015

870

Table 2. Particle diameter, percentile of total PNCs and modal fit parameters for median size distributions at each site. σ is the geometric standard deviation of the mode, N_m is the mode number concentration, $D_{p,m}$ is the geometric mean diameter of the fitted log-normal mode.

Type	Sites	Peak diameter	Number Concentration (cm^{-3})						Fitted mode 1			Fitted mode 2			Fitted mode 3		
		(nm)	Average	5%	16%	50%	84%	95%	$D_{p,m}$ (nm)	N_m (cm^{-3})	σ	$D_{p,m}$ (nm)	N_m (cm^{-3})	σ	$D_{p,m}$ (nm)	N_m (cm^{-3})	σ
Urban	GZ_u	85	13716	5222	6939	11563	20192	29838	166	3078	1.60	65	5404	1.72	17	5621	1.82
	SH_u	40	12931	4195	5903	10560	19746	28986	218	917	1.49	71	5863	1.7	25	4449	1.55
	UR_u	24	28421	6663	10977	22415	45214	70341	146	555	1.89	59	7122	1.83	24	18910	1.73
	WX_u_win	52	19465	5818	8556	16046	29533	47583	142	4972	1.60	63	9878	1.67	29	1250	1.33
	WX_u_sum	73	17396	7710	10572	16051	23794	31408	154	2092	1.61	61	7844	1.6	23	7473	1.59
	JH_u	115	14331	5029	6848	12809	21328	29956	329	206	1.23	116	10753	1.71	36	1892	1.52
Regional	HS_r	72	16076	7548	9635	15084	22230	27898	134	5784	1.61	59	9252	1.63	-	-	-
	KP_r	93	11170	2587	4177	7900	16520	32707	327	311	1.40	95	6883	1.81	17	1280	1.76
	JX_r_sum	68	16593	5320	7799	13033	23059	40126	197	1482	1.56	84	5560	1.56	25	7690	1.86
	JX_r_win	87	13610	3588	5700	11737	20917	30128	138	4946	1.59	74	2460	1.38	38	4451	1.6
	YF_r	123	10195	2259	4033	8761	15610	23455	150	5715	1.83	66	1831	1.58	26	1436	1.56
Coastal/ background	BG_c	90	7163	1885	3233	5874	10401	16519	211	1124	1.50	83	3798	1.66	35	924	1.37
	WL_c	73	5661	992	1659	3941	10207	16108	192	1413	1.63	68	2275	1.63	31	270	1.37
	CD_c	70	6629	1610	2594	5743	10451	14902	148	2247	1.67	57	3479	1.71	-	-	-
Cruise	ES_s	88	5571	1450	2259	4618	8391	17276	132	2123	1.55	59	2484	1.62	-	-	-

874 **Table 3.** Summary of parameters of NPF events at different sites.

Site	Type	Country	Season	CS($\times10^{-2}$ s^{-1})*	GR (nm h^{-1})*	Source
WX_u	Urban	China	Summer	1.7 (0.9-2.8)	10.4 (6.2-13.3)	This study
			Winter	None	None	This study
SH_u	Urban	China	Summer	2.0 (1.0-3.3)	8.0 (4.2-12)	This study
GZ_u	Urban	China	Autumn	3.9 (2.6-5.6)	10.9 (7.3-18.1)	This study
JH_u	Urban	China	Autumn	None	None	This study
UR_u	Urban	China	Spring	1.6 (1.0-2.6)	-	This study
Beijing	Urban	China	Whole year	0.6-6.1	0.1-11.2	(*Wu et al.*, 2007)
Lanzhou	Suburban	China	Summer	1.6 (0.9-2.4)	4.4 (1.4-17.0)	(*Gao et al.*, 2011)
Mexico City	urban	Mexico	Spring	-	0.5-9	(*Dunn et al.*, 2004)
Tecamac	Suburban	Mexico	Spring	-	15-40	(*Iida et al.*, 2008)
New Delhi	Urban	India	Autumn	5-7	15.0 (11.6-18.1)	(*Monkkonen et al.*, 2005)
Budapest	Urban	Hungary	Whole year	1.2	7.2（2.0-13.3）	(*Salma et al.*, 2011)
Po Valley	Urban	Italy	Whole year	1.0 (0.4-1.8)	6.8 (4.2-8.0)	(*Hamed et al.*, 2007)
JX_r	Regional	China	Summer	2.2 (1.1-4.1)	13.6 (7.9-19.6)	This study
			Winter	None	None	This study
YF_r	Regional	China	Summer	2.7 (0.5-5.3)	12.3 (8.6-21)	This study
HS_r	Regional	China	Autumn	None	None	This study
KP_r	Regional	China	Autumn	2.5 (0.3-8.6)	7.4 (3.2-13.5)	This study
Back-garden	Regional	China	Summer	2.6 (2.3-3.3)	12.1 (4.0-22.7)	(*Yue et al.*, 2013)
Xinken	Regional	China	Autumn	-	8.3 (2.2-19.8)	(*Liu et al.*, 2008)
K-puszta	rural	Hungary	Summer	0.5 (0.06-1.4)	6.1 (2.2-14.4)	(*Yli-Juuti et al.*, 2009)
WL_c	Coastal	China	Autumn	2.6	7.5	This study
BG_c	Coastal	China	Autumn	1.4 (1.0-1.8)	4.5 (3.2-7.5)	This study
CD_c	Coastal	China	Spring	2.0 (1.9-2.1)	5.7 (4.5-6.8)	This study

ES_s	Marine	China	Spring	0.9 (0.8-1.1)	2.8 (1.6-3.9)	This study
Shangdianzi	Background	China	Whole year	2	4.3 (0.3-14.5)	(*Shen et al.*, 2011)
Yellow Sea	Marine	China	Spring	-	3.4	(*Lin et al.*, 2007)
Foresthill	Remote	American	Winter	-	2-8	(*Creamean et al.*, 2011)
Hyytiala	Forest	Finland	Whole year	0.2 (0.04-0.8)	3.0 (0.2-12)	(*Maso et al.*, 2005)

* The values outside the bracket represent the average CS or GR; the values inside the bracket represent the maximum and minimum CS or GR observed at each site; "none" means that there is no NPF events found in the whole measurement; "-"means that the GR value can not be calculated (only for the site of UR_u), or there is no such information in the reference paper.

879 **Table 4.** Summary of contribution of NPF events to potential CCN during the time

880 between 14:00 to 17:00 in all measurements.

	Spring		Summer		Autumn		Winter	
	S_c=0.5	S_c=0.2	S_c=0.5	S_c=0.2	S_c=0.5	S_c=0.2	S_c=0.5	S_c=0.2
Urban	33%	6%	66%	26%	31% 0%	9% 0%	0%	0%
Regional	-	-	57% 28%	23% 5%	30% 0%	6% 0%	0%	0%
Coastal	10%	<1%		-	8% 5%	<1% <1%	-	-
Cruise	<1%	<1%	-	-	-	-	-	-

881 "-" represents that there is no measurement at that type of sites in the certain season; "0%" represent
882 that there is no NPF event found in the measurement; "<1%" represent that there are NPF events
883 found in the measurement, but the relative contributions of these NPF events to the total CCN
884 concentration are smaller than 1%.
885
886

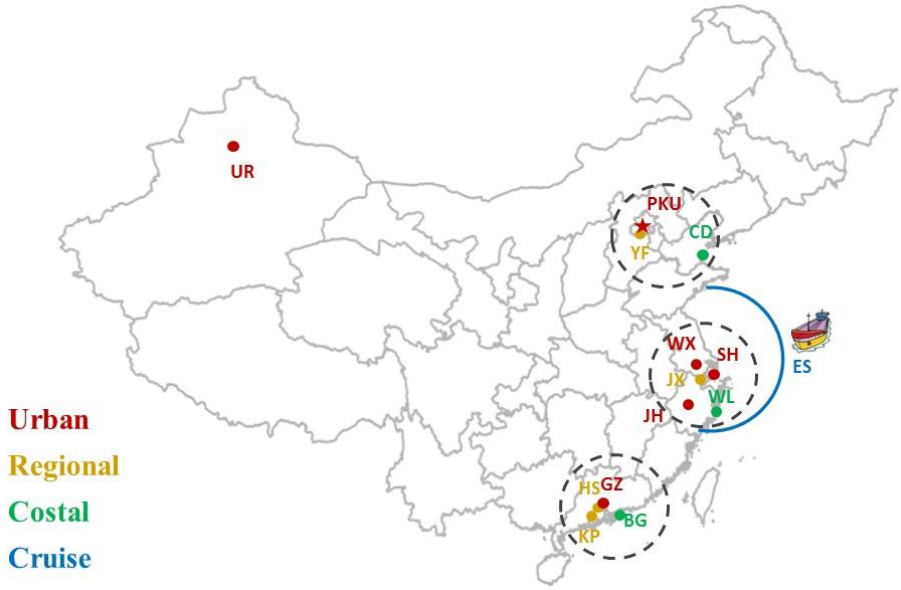

887

888 **Figure 1.** The location of all the thirteen measurement sites. Red, yellow, green and
889 blue color dots represent the site type (urban, regional, costal and cruise. Black circles
890 show the three largest urban areas in China.

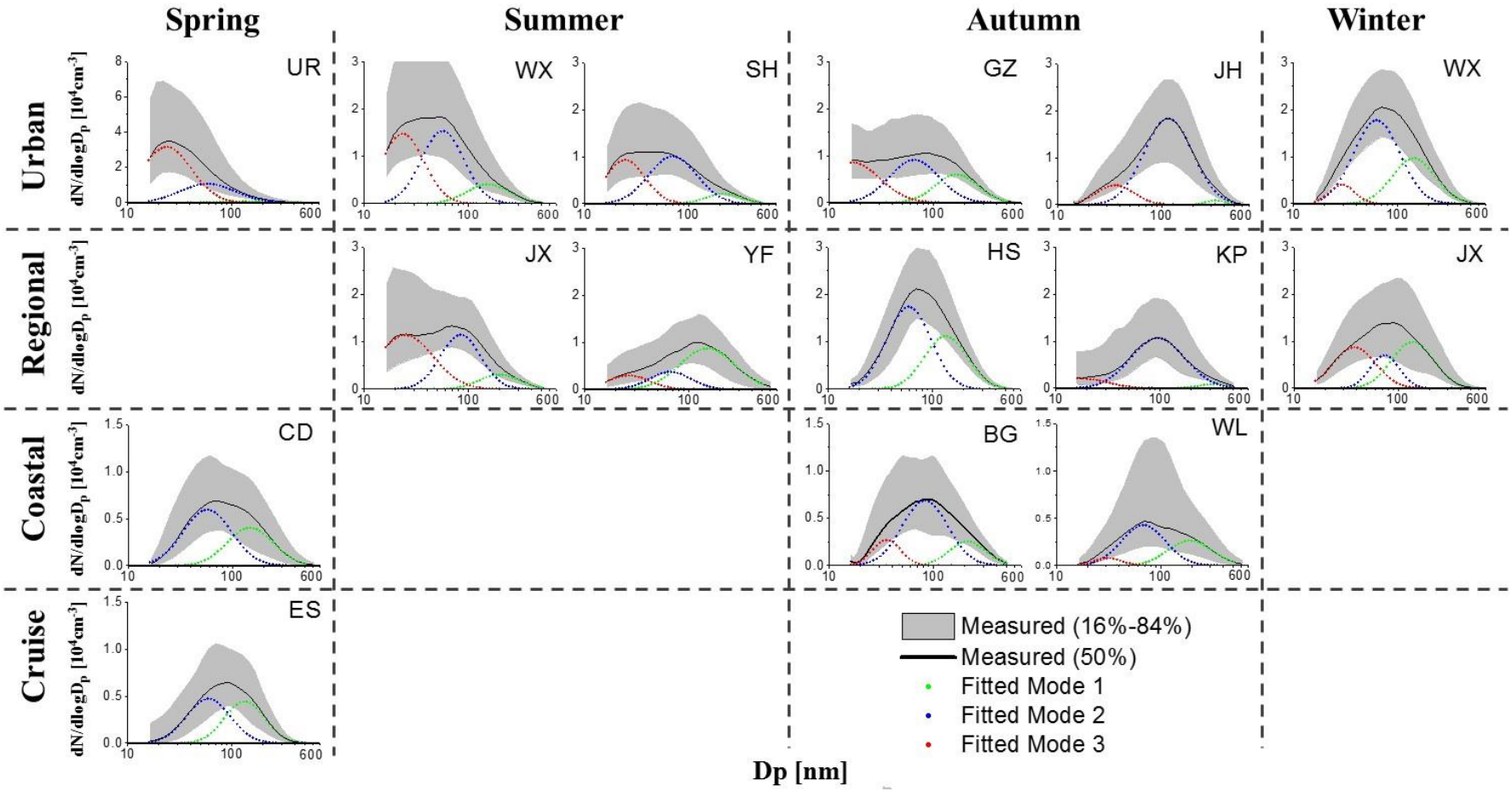

891

892 **Figure 2.** Median distribution (solid black line), 16th and 84th percentile distribution (shaded areas) and fitted mode (green, blue and red scatter

893 dots) at all the measurement sites.

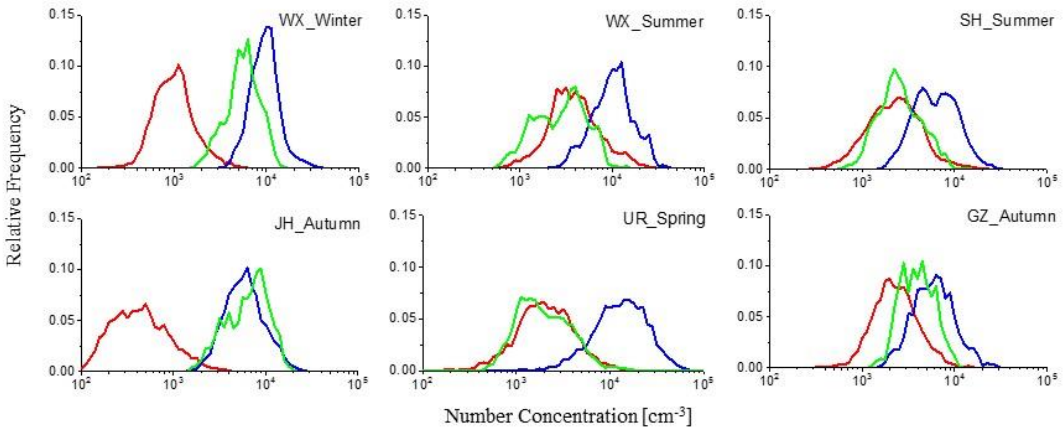

(a)

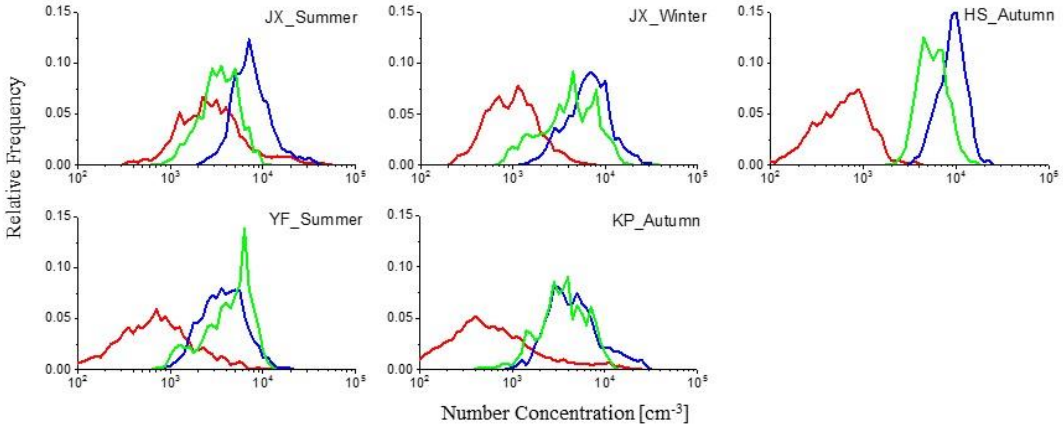

(b)

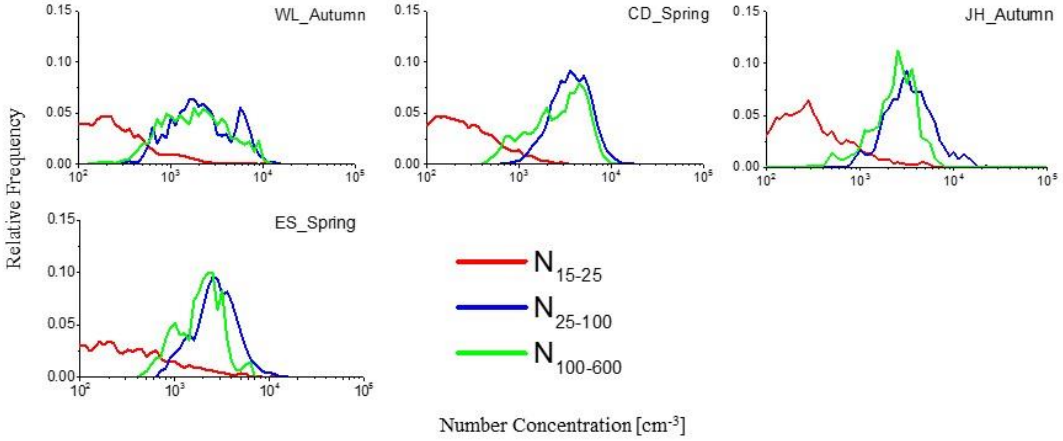

(c)

Figure 3. Distribution of PNC in different size ranges at (a) urban sites, (b) regional sites, (c) coastal sites and ship measurement. The red, blue and green line represents the distribution of $N_{15\text{-}25}$, $N_{25\text{-}100}$ and $N_{100\text{-}600}$, respectively.

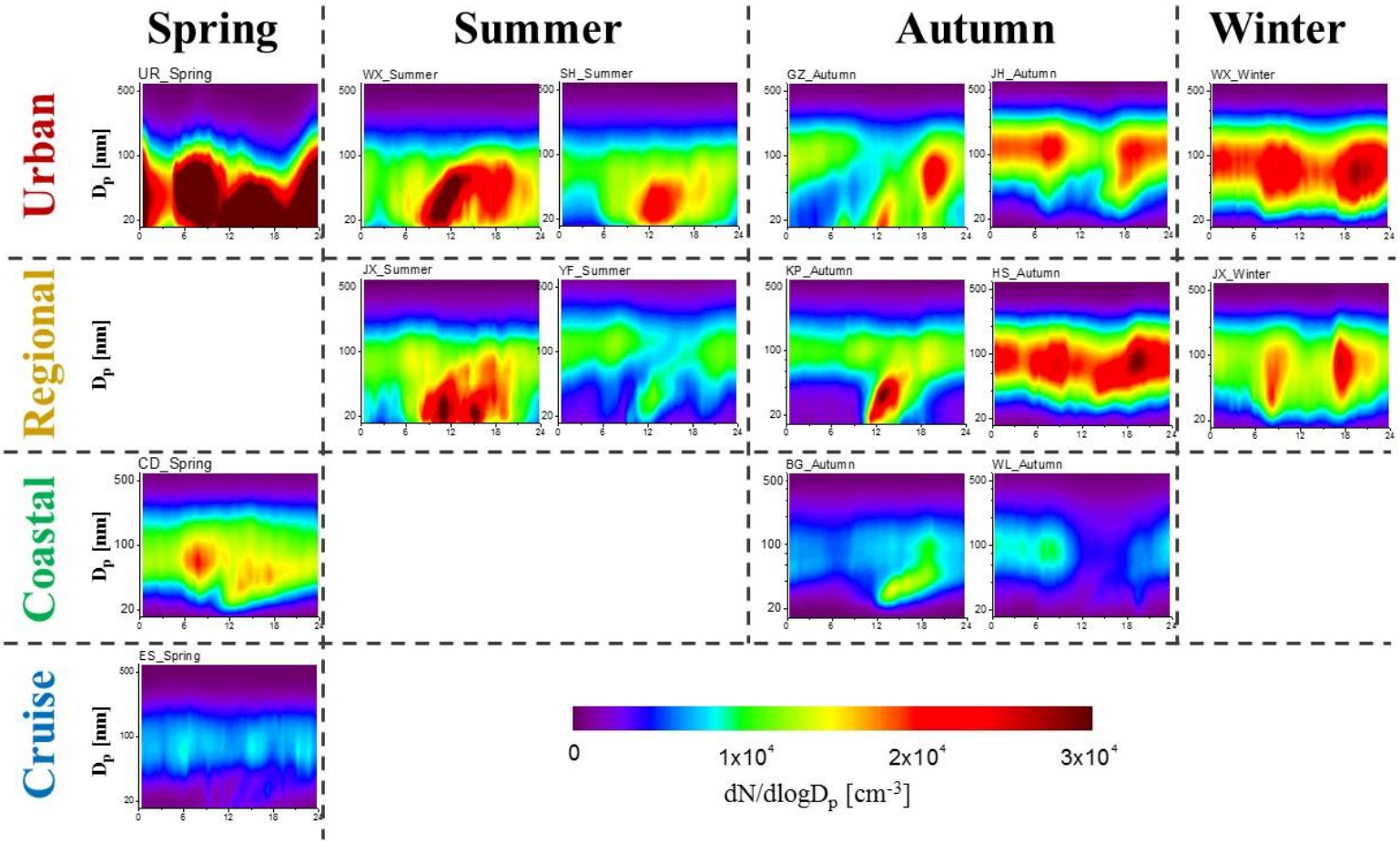

Figure 4. Diurnal variation of PNDs during measurements at different types of sites during different seasons. The color represents dN/dlogDp (cm^{-3}). All diurnal variation figures use the same axis and color bar.

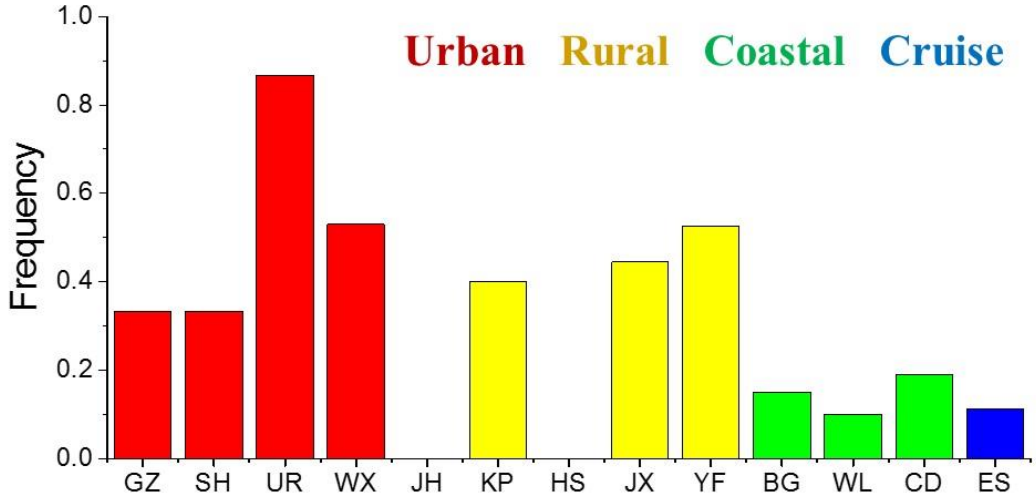

906

907 **Figure 5.** Frequencies of NPF events at different sites. The color of red, yellow, green and blue

908 represent the site type of urban, rural, coastal and cruise, respectively.

909

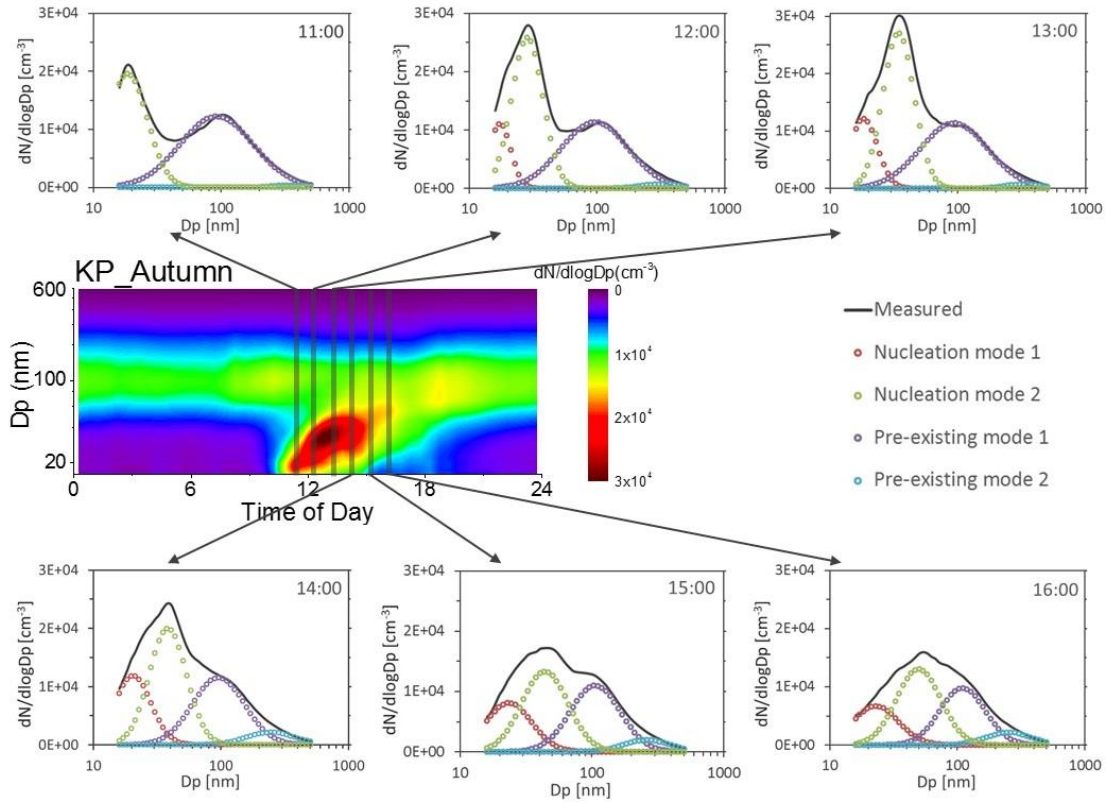

910

911 **Figure 6.** Lognormal fitting result of diurnal average PND at KP_r site. The six line and
912 symbol pictures show the mode fit results for the diurnal variation from 11:00 to 16:00
913 at KP_r site. Totally two nucleation modes and two pre-existing modes are found by
914 mode fitting.